Blunt-Body Problem in Nonuniform Flowfields

T. C. Lin,* B. L. Reeves,† and D. Siegelman†
Avco Systems Division, Wilmington, Mass.

An investigation has been made to study the influence of a nonuniform freestream on blunt-body flowfields. Two different classes of shear flows are considered here, i.e., jet and wake flows. The blunt-body inviscid flow and boundary-layer structure with real-gas properties are examined. Results based on a Navier-Stokes model also are reported. Numerical results indicate that the freestream nonuniformity can alter the blunt-body flow properties significantly. The physical implication of this flow nonuniformity upon ground test data interpretation, flow instability and heating augmentation in debris erosion environments, and pulsating flow on indented nosetips is discussed.

I. Introduction

THERE are several fluid-mechanics problems of current interest where it is necessary to compute the flow about a blunt body in a nonuniform freestream. These problems may be classified into two categories – those where the freestream exhibits a "wake flow" distribution, and those where the freestream shows a "jet" distribution. The shear flow can be essentially parallel or divergent. A typical example of the first class consists of deploying objects (such as a towed decelerator) into the wake of a re-entry vehicle. The freestream shear flow that the decelerator sees is nearly parallel, and the static pressure is nearly constant. However, the nosetip may encounter a highly rotational flow with a severe entropy gradient. Figure 1a depicts a Schlieren photograph[1] of the flowfield around a cylinder that is immersed in the wake of a slender wedge. The distinguishing feature is the existence of a pair of swirling vortices in the stagnation region of the cylinder. The flow properties are completely different from those that pertain when the oncoming stream is uniform.

The second class concerns a blunt body immersed in an expanding flowfield, such as produced by a contoured nozzle or exhaust plume (Fig. 1b). These flows are encountered during the testing of ablative or transpiration nosetips in arc jet facilities. The freestream experienced by the blunt body is a highly underexpanded freejet, which consists of a steep gradient in the flow angle and gas properties in both the radial and axial directions. It is apparent, therefore, that one must understand the nonuniform flow effects before one can interpret the experimental data.

Recently, interest in high-performance re-entry vehicles has led to investigations of the problems of heating augmentation, flow instability induced on indented nosetips (Fig. 2a), and debris erosion (Fig. 2b). These topics have direct and/or indirect connection with nonuniform freestream effects.

Inouye[2] used an inverse method to compute the inviscid flow over elliptical bodies in a spherical source flow. Solutions were restricted to flow divergence of a few degrees. Crowell[3] used the method of integral relations to calculate flowfields corresponding to two different types of freestream, i.e., a source flow and the exhaust plume from a contoured nozzle. Since a one-strip integral method is used, his formulation is restricted to flows with small deviation from a uniform flow. Moore et al.,[4a] Bordner and Davis,[4b] and Black, et al.[4c] carried out a series of numerical calculations to demonstrate the effects of nonuniform freestream over a sharp and blunt cone. Some interesting results due to crossflow are noted. Also, they have found that boundary-layer separation is possible in the case of a wake flow. Recently, Schmidt[12] modified Moretti's[5] program to investigate a shear flow over a blunt body at incidence. His formulation is for the inviscid flow only.

It is the purpose of this paper to present a general formulation for calculating the flowfield around a blunt body immersed in a nonuniform freestream. No restriction on the degree of nonuniformity will be imposed on the oncoming stream. Both viscous and inviscid flow calculations have been carried out, and comparisons with experimental data are given. The definition of the freestream distribution is given in Sec. II. A brief discussion of the numerical formulation for the inviscid flow and boundary layer is described in Sec. III. Numerical results are discussed in Sec. IV. Some results for wake flows, based on a Navier-Stokes model, are presented in Sec. V. Finally a brief summary is given in Sec. VI.

II. Definition of Freestream Flowfield

Two types of nonuniform freestream are studied here. The first type concerns freejet flowfields, i.e., a blunt body immersed in the exhaust plume of an underexpanded nozzle (Fig. 1b). Figure 3a illustrates the flow profiles[11] at a small distance away from the nozzle exit. It clearly indicates a steep gradient in the flow properties. For example, the pitot pressure varies almost 300% from the centerline (i.e., $y=0$) to $y=0.7$ in. It should be noted that, to date, the arc heater has been the most successful ground test facility in producing an environment for testing ablative materials for re-entry vehicles. Therefore, it is important to understand the effect of this type of flow nonuniformity upon heat-transfer, surface pressure, and transition phenomena before one can interpret the experimental data.

The second class of nonuniform freestream corresponds to a wake-type shear flow. The flow profiles are described by the following relation:

$$U_\infty(y)/U_\infty(\infty) = 1 - a\exp(-by^2), \quad v=0$$

or, alternatively,

$$U_\infty(y)/U_\infty(0) = 1 + A_1(y/B_1)^2, \quad y \le B_1 \tag{1a}$$

$$U_\infty(y)/U_\infty(0) = 1 + A_1, \quad y > B_1 \tag{1b}$$

$$p_\infty(y)/p_\infty(0) = 1 \tag{1c}$$

$$h_\infty(y)/h_\infty(0) = 1 + C\{1 - [U_\infty(y)/U_\infty(0)]^2\} \tag{1d}$$

Presented as Paper 76-354 at the AIAA 9th Fluid and Plasma Dynamics Conference, San Diego, Calif., July 14-16, 1976; submitted Sept. 2, 1976; revision received May 2, 1977.

Index categories: Jets, Wakes, and Viscid-Inviscid Flow Interactions; Nonsteady Aerodynamics.

*Staff Scientist; presently at The Aerospace Corporation, El Segundo, Calif. Member AIAA.

†Staff Scientist. Member AIAA.

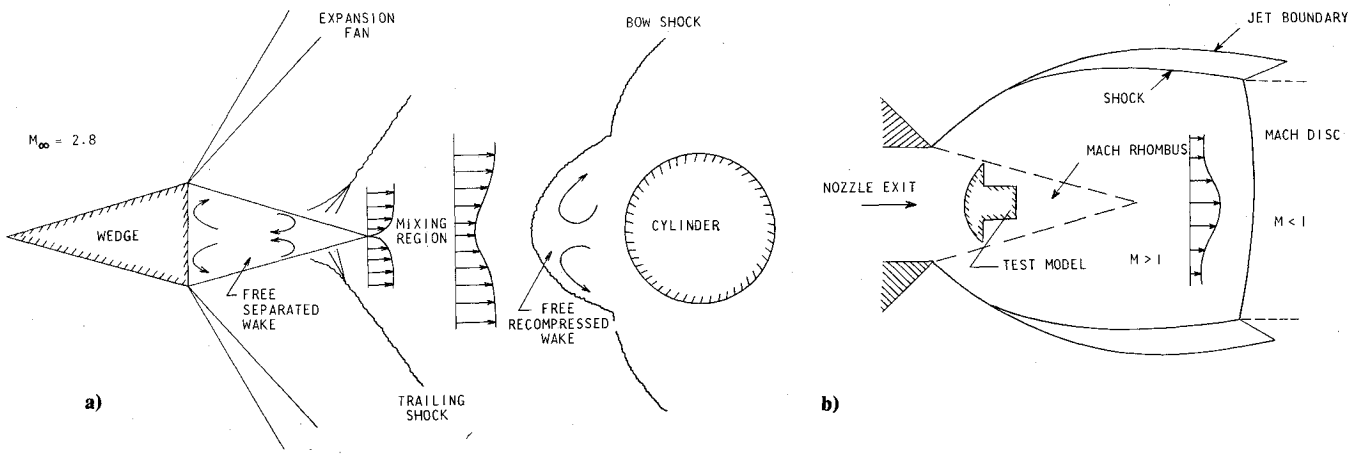

Fig. 1 a) Schematic configuration of a free cavity (turbulent wake); b) schematic of an underexpanded jet.

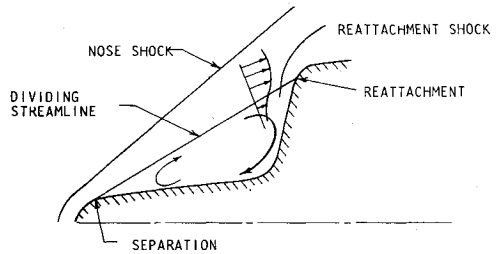

Fig. 2a Flow over a spiked bluff body: shear layer.

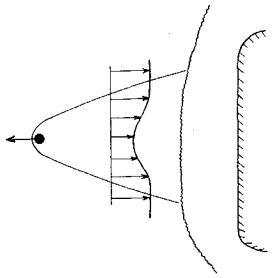

Fig. 2b Particle ejecta: wake.

where $U_\infty(\infty)$ is the wake velocity as $y \to \infty$. A_1, B_1, a, b, and c are parameters related to the strength and width of the wake. When $C = (\gamma - 1)/2M_\infty^2(0)$, a freestream shear flow with constant total enthalpy is imposed. Flow profiles with $C \neq 0$ will exhibit an entropy gradient.

III. Formulation

A. Inviscid Flow

The inviscid flowfield is calculated from Moretti's time-dependent blunt-body code,[5-7] which has been modified to include nonuniform freestream and real-gas (equilibrium air) effects.[8] In Moretti's formulation, the interior points are integrated by MacCormack's two-level explicit scheme.[9] The outer bow shock is treated as a sharp discontinuity, and the Rankine-Hugoniot conditions are imposed there. The effects of freestream nonuniformity appear in the calculation of the shock points. The boundary conditions at the wall are treated by a modified method of characteristics.[5]

B. Boundary-Layer Calculations

In order to compute the effects of freestream nonuniformity upon the local boundary-layer properties, an existing integral matrix method[10] was modified suitably. This code considers laminar and turbulent flows for arbitrary chemical systems in thermochemical equilibrium. The computer program was modified suitably to include the effects of variable total enthalpy and entropy layer entrainment.

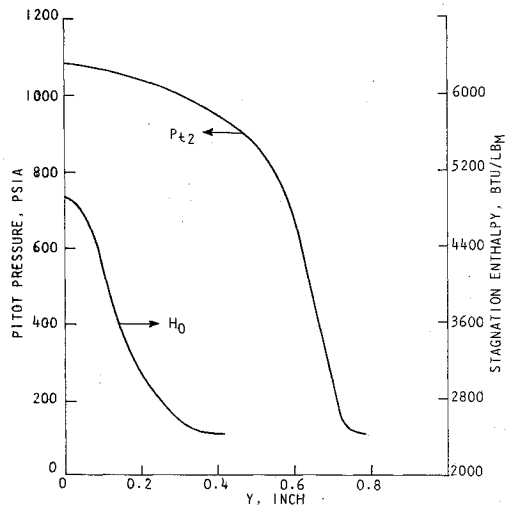

Fig. 3a Arc heater freestream profiles.[11]

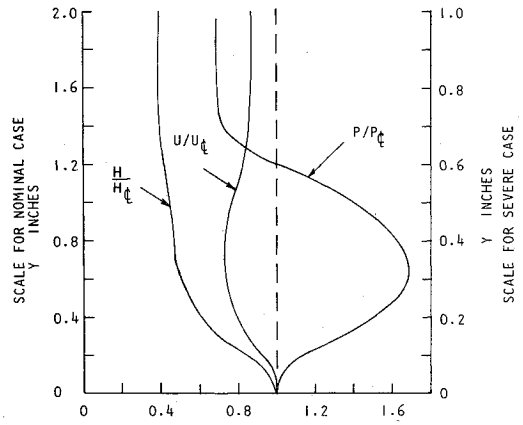

Fig. 3b Arc heater freestream profiles.[11]

IV. Discussion of Results

A. Freestream with "Jet" Distribution

The specific type of shear flow considered here is characterized by the appearance of large total enthalpy gradient. A distribution of H_0 obtained in an arc heater[11] is shown in Fig. 3a. The stream is highly rotational, and the corresponding flow profiles are given in Fig. 3b. These spiked profile distributions are believed to be caused by incomplete mixing between the hot arc heater core and the cool diluent gas. Since the gas is hot (the stagnation enthalpy at the centerline is of the order of 6000 Btu/lb), it is necessary to carry

out a real-gas calculation. In order to assess the sensitivity of the results to the degree of nonuniformity, a second set of freestream flow profiles (Fig. 3b) with steeper gradients also has been used. We shall refer to the latter distribution as the severe case and the former one as the nominal case.

Figure 4 depicts the effects of freestream nonuniformity upon the bow shock distribution for a spherical nosetip. The sonic point locations also are shown in the figure. The shock standoff distance tends to decrease as the degree of freestream nonuniformity becomes stronger. The behavior of the shock standoff distance can be inferred from one-dimensional stream tube continuity considerations.[11] Predicted surface pressure distributions are given in Fig. 5 and are compared with experimental data.[11] A faster reduction in the wall pressure level is discerned when the freestream becomes nonuniform.

The effects of freestream nonuniformity upon the local boundary-layer properties are demonstrated in Figs. 6 and 7. An increase in the velocity gradient ($\partial U/\partial s$) in the case of a shear flow is noted. This effect results in a higher heating rate near the stagnation point. This is apparent from the reduction in the shock standoff distance, which causes the sonic point to move inward. This result is significant for the interpretation of experimental stagnation-point heat transfer $\dot{q}_s$. With a uniform freestream, the velocity gradient is inversely proportional to the nose radius, i.e.,

$$\frac{\dot{q}_s}{\rho_\infty U_\infty (H_0 - h_w)} \sim \sqrt{\frac{\mu_s}{\rho_\infty U_\infty r}} \tag{2}$$

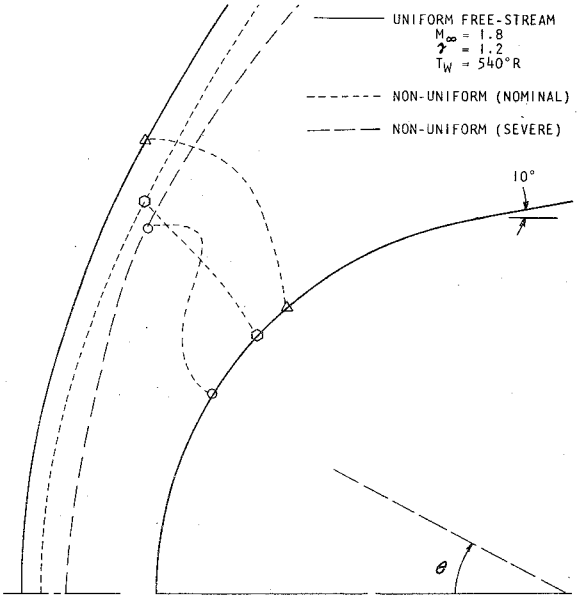

Fig. 4 Shock shape on spherical nosetip.

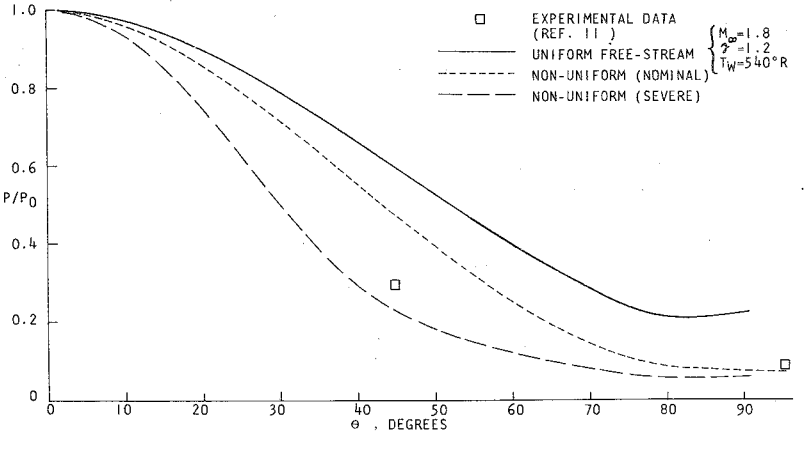

Fig. 5 Pressure distribution on sphere.

This is not the case for nonuniform flow; a simple correlation of $\dot{q}_s$ with the radius of the sphere is invalid in a shear flow. Also, the laminar heat flux downstream of the sonic point decreases faster in a nonuniform flow. This tendency essentially reflects the lower level of the surface pressure. Comparisons of experimental heat-transfer measurements with the theoretical predictions for laminar and turbulent flows are demonstrated in Figs. 6a and 6b.

Figure 7 shows the laminar momentum thickness distribution. Unlike other flow properties, it is noted that θ is relatively insensitive to the presence of the freestream nonuniformity. This can be explained by considering the laminar similarity solution:

$$\theta = \frac{(2\xi)^{1/2}}{\rho_e U_e r_b} I_2(\beta, g_w), \quad \xi = \int \rho_w \mu_w U_e r_b^2 ds \tag{3}$$

The decrease in static pressure level will cause a decrease in density, and it results in a thickening in θ. However, this effect is counterbalanced by the more favorable pressure gradient β and higher edge velocity. Figure 7 depicts the momentum thickness Reynolds number. It shows that Re_θ also is insensitive to the freestream nonuniformity. This again can be explained in terms of counterbalancing effects of higher edge velocity, lower edge temperature, and density. These results with respect to θ and Re_θ are interesting because boundary-layer transition in the nosetip region has been correlated in the form

$$Re_\theta = f(K/\theta, T_w/T_s) \tag{4}$$

where K is roughness height. Therefore, transition from laminar to turbulent flow is predicted to be relatively insensitive to freestream nonuniformities. Further investigations examining the effects of roughness are needed to confirm this observation.

B. Freestream with "Wake Flow" Distribution: Inviscid Flow

The velocity distribution in the freestream has been assumed to have either an exponential or parabolic form. The density profile varies in the radial direction, whereas the static pressure remains constant [see Eq. (1)]. Here a flow picture completely different from the previous case of "jet flow" is observed. For example, the shock standoff distance Δ near the stagnation point is larger than for the case of uniform flow. It is noted that, as $A_2 = U_\infty(\infty)/U_\infty(0) = 1.2$, $C = 1.085$, a 45% increase in Δ at the stagnation point is realized. This phenomenon, together with the aft movement of the surface sonic point, will result in a reduction of stagnation-point heat transfer.

The pressure distribution on the body surface is given in Fig. 8. The freestream nonuniformity causes the wall pressure to be fairly constant and equal to the stagnation pressure. However, the static pressure behind the bow shock can in-

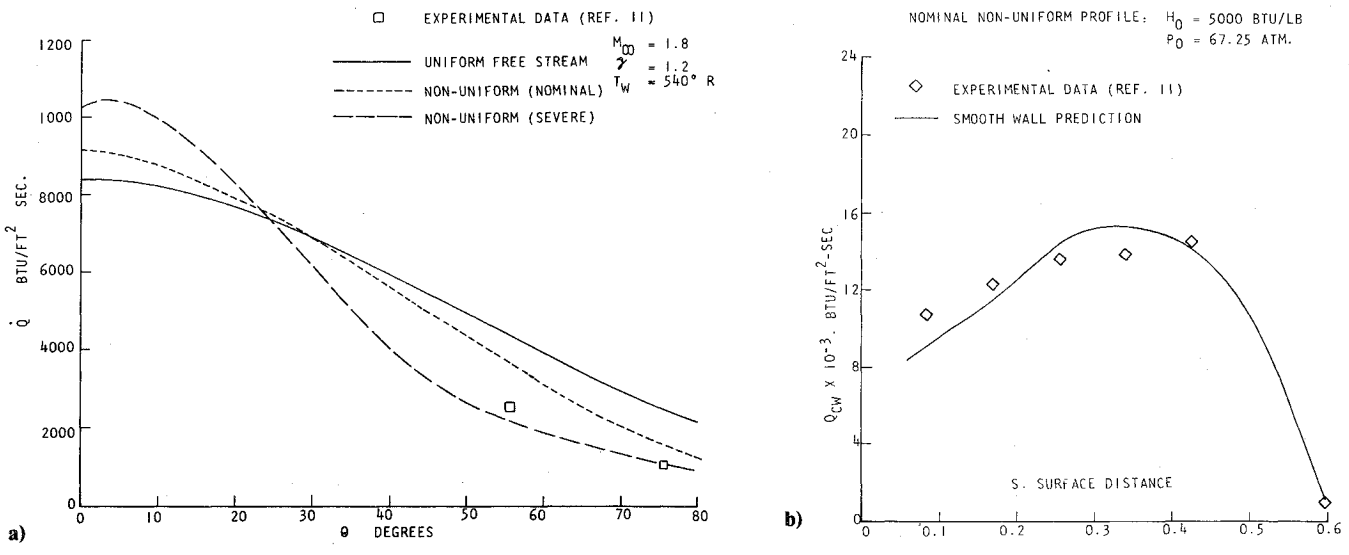

Fig. 6 a) Laminar heat transfer on sphere; b) turbulent heat transfer on blunt model.

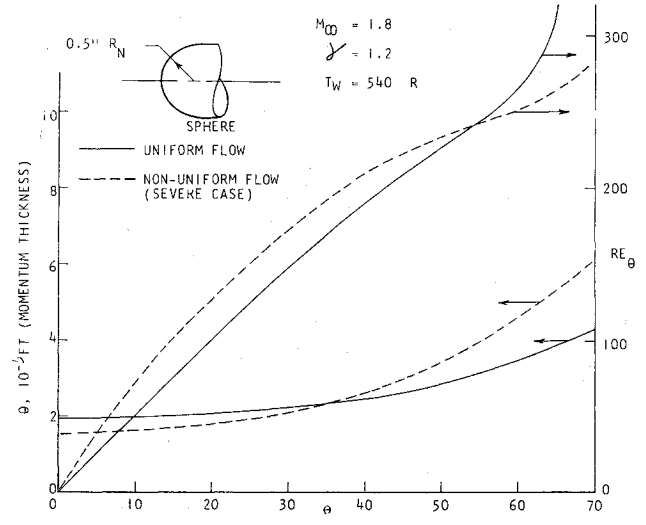

Fig. 7 Momentum thickness and Re_θ distribution.

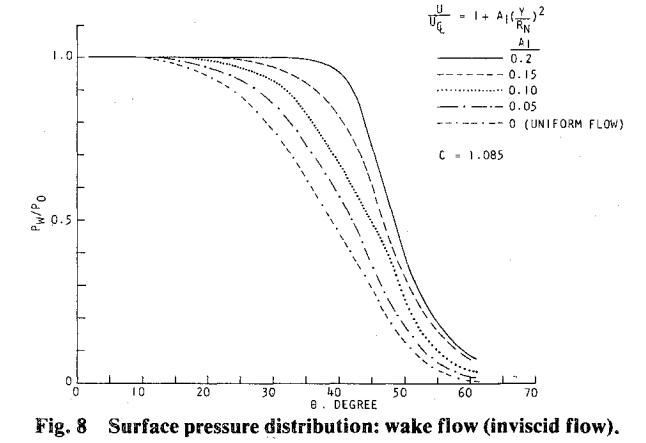

Fig. 8 Surface pressure distribution: wake flow (inviscid flow).

crease away from the centerline when the degree of nonuniformity is sufficiently strong (Fig. 9). For the local subsonic flow, this adverse pressure gradient can be severe enough to induce flow reversal. Indeed, this is found in the present numerical results. A plot of velocity vectors is demonstrated in Fig. 10 for $A_1 = 0.2$ and $C = 1.085$. It clearly shows the formation of a pair of vortices behind the bow shock. The reattachment point is located near the shoulder, whereas at the stagnation point on the blunt body the flow direction is away from the body surface. A second stagnation point is found along the centerline in the shock layer off the body surface. The Charwat, et al. Schlieren photograph[1] of a cylinder immersed in the wake of a slender wedge confirms the existence of such a pair of vortices.

When the nonuniformity becomes stronger, convergent steady solutions cannot be found. Instead, oscillations in bow shock position and flow properties (such as surface pressure) develop. This is demonstrated in Fig. 11. Thus, the numerical inviscid flow results suggest that a freestream shear flow with a "wake" distribution tends to destabilize the flow.

The appearance of the separated flow makes the inviscid flow calculation suspect. In order to verify the existence of this recirculation flow region, calculations with the Navier-Stokes equations were carried out. These are reported in the next section.

V. Freestream with "Wake Flow" Distribution: Navier-Stokes Model

Moretti and Salas' formulation[13] is modified here to evaluate the effects of a shear flow. The Navier-Stokes equations in spherical coordinates are

$$f_t + N_1 f_r + N_2 f_\theta + N_3 = (1/Re)h$$

where

$$f = \begin{bmatrix} p \\ u \\ v \\ s \end{bmatrix}; \quad N_1 = \begin{bmatrix} u & \gamma & 0 & 0 \\ T & u & 0 & 0 \\ 0 & 0 & u & 0 \\ 0 & 0 & 0 & u \end{bmatrix} \tag{5a}$$

$$N_2 = \frac{1}{r}\begin{bmatrix} v & 0 & \gamma & 0 \\ 0 & v & 0 & 0 \\ T & 0 & v & 0 \\ 0 & 0 & 0 & v \end{bmatrix}; \quad N_3 = \begin{bmatrix} (2U + v\cot\theta)\gamma \\ -v^2 \\ uv \\ 0 \end{bmatrix}\frac{1}{r} \tag{5b}$$

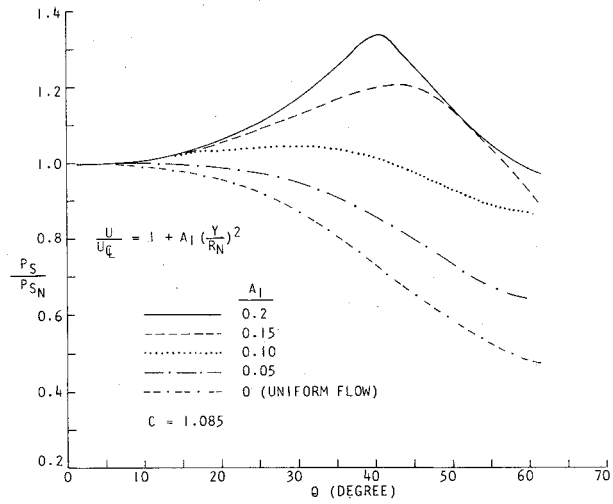

Fig. 9 Pressure behind the shock: wake flow (inviscid flow).

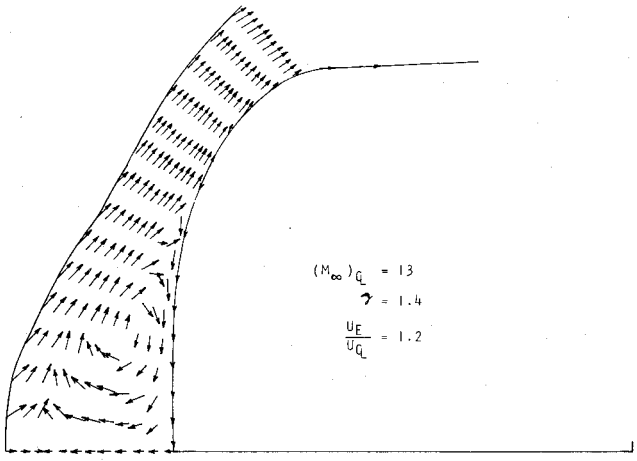

Fig. 10 Velocity field near an ellipsoid: inviscid flow model.

$$h = \begin{bmatrix} \beta_1\phi + \beta_2 \nabla \cdot (\mu \nabla T) \\ \beta_2 H_2 \\ \beta_3 H_3 \\ \beta_1\phi + \beta_2 \end{bmatrix} \tag{5c}$$

where

$$\beta_1 = \sqrt{\gamma}(\gamma-1)M_\infty/p$$

$$\beta_2 = {}_{\gamma}3/2\, M_\infty/p_r P$$

$$\beta_3 = \sqrt{\gamma} M_\infty/\rho$$

ϕ = dissipation function

and where

$$H_2 = \tfrac{1}{3}\{4U_{rr} + [8U_r + V_{r\theta} + V_r \cot\theta + (3U_{\theta\theta} - 8U - 7V_\theta + (3U_\theta - 7V)\cot\theta/r)]/r\}$$

$$H_3 = \tfrac{1}{3}\{3V_{rr} + [U_{r\theta} + 6V_r + 4(2U_\theta + V_{\theta\theta} + V_\theta \cot\theta - V\sec^2\theta)/r]/r\}$$

A transformation of the coordinate system from (t,r,θ) to (t,η,θ) is performed, i.e.,

$$\zeta = (r - r_b)/(r_s - r_b) \tag{6a}$$

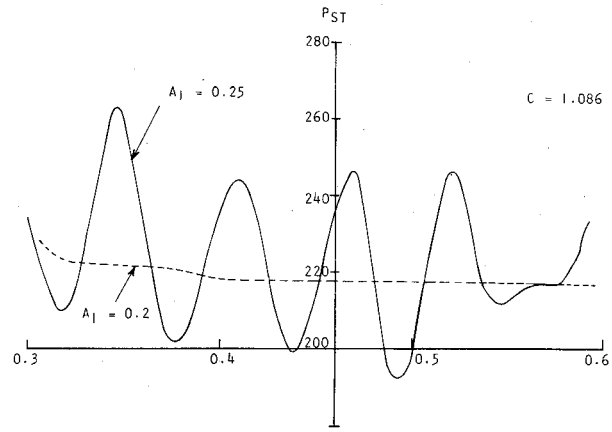

Fig. 11 Stagnation pressure history for inviscid flow.

$$\eta = 1 + \frac{1}{2\alpha} \ln \frac{1 + (\zeta - 1)\tanh \alpha}{1 - (\zeta - 1)\tanh \alpha} \tag{6b}$$

where α is a stretching parameter. Its purpose is to map equally spaced nodes on the η axis near $\eta = 0$ to concentrated nodes on the r axis near the body.

The interior points are integrated by MacCormack's two-level explicit scheme. The shock is treated as a discontinuity, and the same computational routine employed in the inviscid blunt-body problem is used here. This is a good approximation for high Reynolds number flow. An isothermal wall with no-slip boundary conditions is imposed at the wall. The surface pressure is calculated from the following relation:

$$p_t + \eta_\zeta \zeta_r \gamma (U_\eta - r_{b_\theta} V_\eta / r_b) = (1/Re)h \tag{7}$$

Equation (7) is treated in a similar way as for interior points, and the η derivatives of u and v are approximated by a second-order end difference formula. Sample calculations with $p_\eta = 0$ at the wall have been made. For high Reynolds number flow, no significant difference is observed between results from these two ways of handling wall points.

Numerical results are presented here for hypersonic flow over a sphere ($R_N = 1$ in.). The freestream centerline Reynolds number is $Re_\infty = \rho_\infty(0)U_\infty(0)R_N/\mu_\infty(0) = 5000$, Mach number $M_{\infty_t} = 10$, and wall temperature ratio $T_w/T_0 = 0.1$. The bow shock distribution is given in Fig. 12. The position of the sonic lines also are shown in this figure. Compared to the results for a uniform freestream, the shock extends farther upstream near the centerline and possesses larger curvature. The latter behavior can be explained by a higher density and velocity off the centerline in the nonuniform flow case. When the wake parameter $a = 0.04$ and $c = 3.0$, we find that the centerline shock standoff distance $\Delta = 0.168$. As a increases to 0.065, the shock moves upstream to $\Delta = 0.24$, which is almost twice the value in a uniform flow. At these conditions, the shock exhibits a convex-concave shape.

The surface pressure distributions are shown in Fig. 13. According to the Navier-Stokes solution, the peak pressure appears off the centerline. In the inviscid flow calculations, the wall is treated as a streamline, along which the entropy is a constant, and the surface pressure cannot exceed the centerline stagnation pressure $p_{s,0}$. In the Navier-Stokes calculation, the pressure overshoot can be 5% higher than $p_{s,0}$ when the wake parameter $a = 0.04$, $c = 3.0$, and the surface pressure overshoot increases to 20% as $a = 0.065$ because of viscous mixing. Charwat, et al's experimental data[1] for wakes and Donaldson's freejet impingement measurements[18] show a qualitatively similar trend.

The adverse pressure gradient can be severe enough to cause flow reversal. For example, Fig. 14 illustrates the velocity vector projection. A pair of vortices is found near the

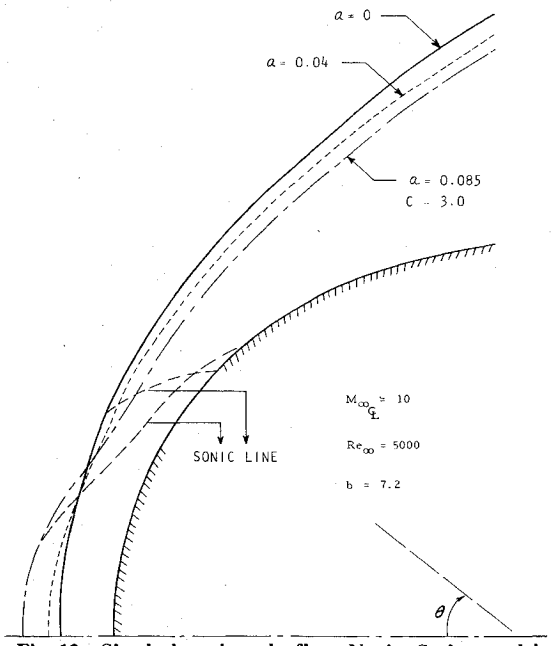

Fig. 12 Shock shape in wake flow: Navier-Stokes model.

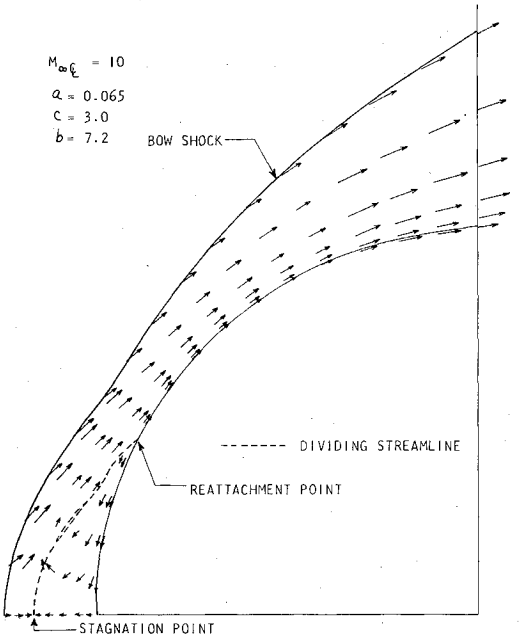

Fig. 14 Flow velocity vector projection: Navier-Stokes model.

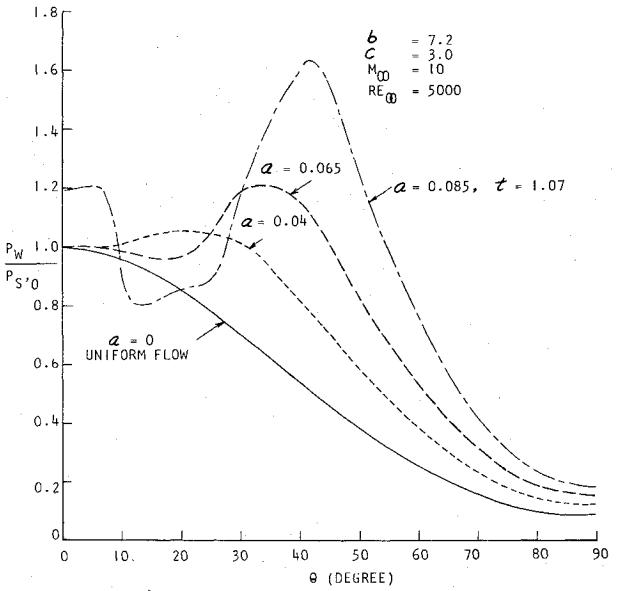

Fig. 13 Surface pressure distribution: Navier-Stokes model.

stagnation region. The separated flow occupies almost 65% of the shock standoff distance along the centerline. The position of the dividing streamline also is given in Fig. 14. The existence of a separation bubble and an effective body approximately equal to the contour of the dividing streamline cause the inflected shock shape shown in Fig. 12.

The laminar surface heat-transfer distribution is shown in Fig. 15. Peak heating occurs away from the stagnation point in the reattachment region. For $a=0.085$, $c=3.0$, the heating overshoot can be 32% higher than the uniform flow stagnation value. Figure 15 also indicates that the stagnation-point heat transfer $\dot{q}_s$ in wake flow is lower than the heating in uniform flow. This is expected, since temperature gradients are small in the separated bubble. Similar results have been measured in flow over spiked bodies.[17]

As a freestream nonuniformity becomes stronger, numerical results with a steady-state condition (i.e., $\partial(\ )/\partial t = 0$) no longer are obtained. Instead, an oscillatory flow pattern develops. Figure 16 demonstrates this unsteady behavior for stagnation pressure. The Strouhal number fD/U_∞, based on one cycle of oscillation, assumes a value of 0.29 for $a=0.085$, $c=3$, and $Re=5000$. Further work is needed to confirm these results for the effect of a on frequency.[14]

In certain periods of the transient flow, both the surface pressure and heating overshoot off the centerline become more pronounced, and the separated bubble grows. This causes the shock to move even farther upstream and results in a higher effective freestream Mach number in shock-fixed coordinates, which produces even larger pressure overshoots. The growth of the bubble and upstream propagation of the shock evidently continue until the bubble is vented to the sidewall pressure as the reattachment point moves downstream around the shoulder.

The unsteady flow behavior predicted by the Navier-Stokes model helps explain the flow instability and heating augmentation phenomenon observed in particle-laden flows over a blunt body and in flows over highly indented nosetips. Particle-induced oscillatory flows are produced by a debris wake when a rebounding particle penetrates the bow shock of a blunt body. The entropy wake behind the particles can extend thousands of particle diameters downstream. According to the present results, instability is determined by the strength of this entropy wake at the shock of the blunt body. The wake axis flow properties for several hundred diameters downstream of a particle can be computed by expanding the shock layer gas ahead of a particle back to freestream pressure isentropically. Figure 17 shows that at hypersonic speeds the inviscid wake-axis Mach number is considerably less than the freestream Mach number. These results are in excellent agreement with Behrens measurements of wake properties 200 diameters downstream of a fine wire at $M_\infty=6$.[15] From Fig. 17, when $M_\infty(\infty)=10$, the Mach number ratio between radial "infinity" and the centerline is $M_\infty(\infty)/M_\infty(0)=2.6$. According to the present numerical results for a sphere, when $M_\infty(\infty)/M_\infty(0)=1.7$, $Re_\infty=5000$, and $T_w/T_0=0.1$, the flow is already unstable.‡ Since the entropy wake can extend many thousands of diameters downstream of a blunt particle, it is evident that unsteady oscillations will occur in particle-laden flows even when the debris size is very small. Of course, in an actual flow, as the bow shock propagates upstream into the wake of a particle the wake profile upstream of the shock must be considered as a function of x, y, and t, i.e., $M_\infty = f(x,y,t)$.

‡Perhaps a nondimensional parameter such as $R^* \ \partial/\partial r\ (M_\infty^2 \sin^2\theta_b)$, can be used to measure the flow nonuniformity.

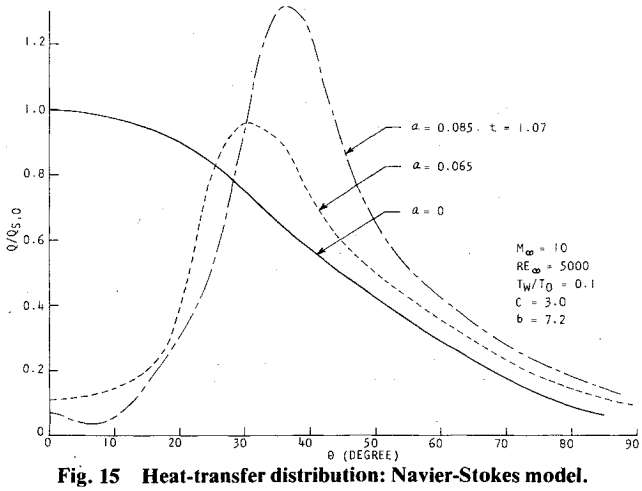

Fig. 15 Heat-transfer distribution: Navier-Stokes model.

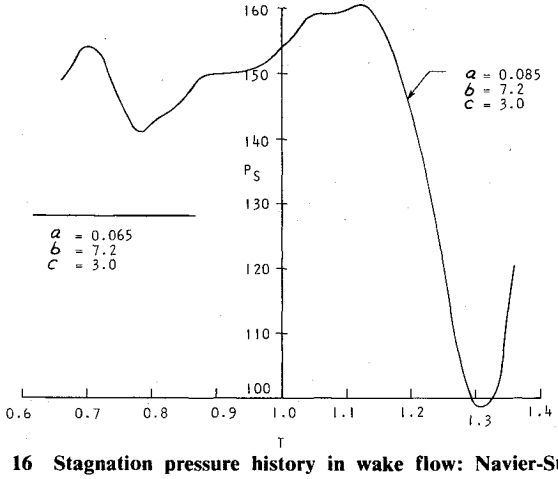

Fig. 16 Stagnation pressure history in wake flow: Navier-Stokes model.

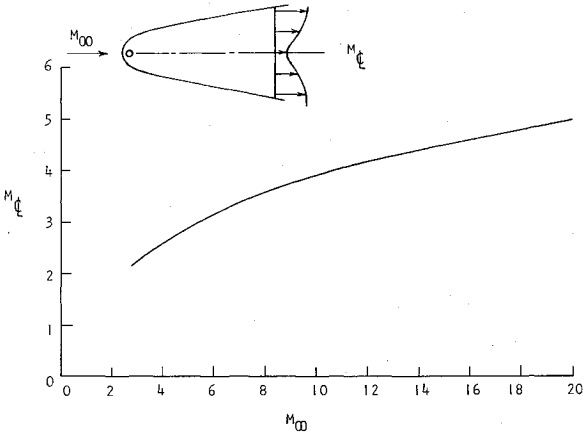

Fig. 17 Inviscid far-wake Mach number on wake axis as function of freestream Mach number.

For flow over an indented nosetip, the analysis of Ref. 16 showed that when the vorticity in the separated shear layer just upstream of the detached reattachment shock at the shoulder becomes too large, strong transverse pressure gradients are produced behind the shock. This drives mass from the shear layer into the recirculation region, and the cavity becomes unstable. The present numerical results provide conclusive evidence that such vortical wake and shear layer flows indeed may become unstable upon passage through a strong shock, and provide quantitative results for conditions at which these instabilities occur.

VI. Summary

A theoretical investigation of nonuniform freestream effects on blunt-body flowfields has been made. Results are presented for two types of shear flows, i.e., wake and jet flows. The numerical results indicate that freestream nonuniformities can alter the flow character and properties significantly, especially when the freestream has a wake profile.

For an oncoming stream with a "jet" flow distribution, the effect is to decrease the surface pressure, move the sonic point closer to the stagnation point, reduce the shock standoff distance, and increase the stagnation-point heat transfer. Preliminary analysis reveals that transition from laminar to turbulent flow is relatively insensitive to the freestream nonuniformity.

A freestream with a "wake" distribution can result in radical changes in the flowfield. When the strength of the shear flow is weak, the bow shock standoff distance is larger and the stagnation-point heat transfer is lower than for uniform flow. As the degree of nonuniformity increases, a pair of vortices appears in the stagnation region. Local maxima in surface pressure and heating occur off the centerline in the region of shear layer reattachment. Moreover, the shock exhibits a convex-concave shape. Finally, when the degree of nonuniformity is strong enough, the blunt-body flowfield becomes unstable. These results help explain certain unsteady flow phenomena that occur in supersonic flow over indented nosetips and in hypersonic particle-laden flow over blunt bodies.

Based on our experience with the numerical calculations, we suggest that it is an appropriate procedure to divide the flowfield into distinct viscous and inviscid flow regions when the freestream shear flow is of a "jet" type. However, this procedure may be inadequate when the oncoming shear flow is of the "wake" type. This is because of the appearance of large separation bubbles near the centerline and substantial overshoots in pressure and heating near reattachment. The predictions of Strouhal number, heat-transfer level, and surface pressure overshoot from the Navier-Stokes model are in qualitative agreement with experimental data for similar types of flows, such as flow over spiked bodies.[1,17,18]

Acknowledgment

This work was supported in part by the Space and Missile Systems Organization under Contract Nos. FO4701-72-C-0150 and F04701-74-C-0208. The authors wish to thank G. Moretti for many valuable discussions.

References

[1] Charwat, A.F., Ross, J.N., Dewey, C.F., Jr., and Hitz, J.A., "An Investigation of Separated Flows – Part I: The Pressure Field," *Journal of the Aerospace Sciences,* Vol. 28, June 1961, pp. 457-470.

[2] Inouye, M., "Numerical Solutions for Blunt Axisymmetric Bodies in a Supersonic Spherical Source Flow," NASA TN-D 3382, April 1966.

[3] Crowell, P.G., "The Blunt Body Problem in an Expanding, Nonuniform Flow Field," Aerospace Rept. TR-0059(S6816-76)-2, SAMSO-TR-70-302, July 3, 1970.

[4] a) Moore, F.G., DeJarnette, F.R., and Brooks, E.N., Jr., "Supersonic Flow of Nonuniform Freestream Past Aerodynamic Decelerations," *Journal of Spacecraft and Rockets,* Vol. 8, Dec. 1971, pp. 1169-1175. b) Bordner, G.L. and Davis, R.T., "Compressible Three-Dimensional Laminar Boundary Layer on Cones at Incidence to Shear and Axisymmetric Wake Flow," Aeronautical Research Lab., ARL 71-0262, Wright-Patterson Air Force Base, Ohio, 1971. c) Black, R.R., Frieders, M.C., and Lewis, C.H., "A Computerized Analysis of Supersonic Nonuniform Flows over Sharp and Spherically Blunted Cones at Angle of Attack," *Journal of Computers and Fluids,* 1973, pp. 359-363.

[5] Moretti, G. and Abbett, M., "A Time-Dependent Computational Method for Blunt Body Flows," *AIAA Journal,* Vol. 4, Dec. 1966, pp. 2136-2141.

[6] Lin, T.C. and Rubin, S.G., "A Two-Layer Model for Coupled Three-Dimensional Viscous and Inviscid Flow Calculations," AIAA Paper 75-853, Hartford, Conn., June 1975.

[7] Boger, R., "Development of Real Gas, Blunt Body Flow Field Program," Avco Corp., K200-TR-72-50, April 18, 1972.

[8] Bade, W.L., "Simple Analytical Approximation to the Equation of State of Dissociated Air," *ARS Journal,* Vol. 29, April 1959, pp. 298-299.

[9] MacCormack, R.W., "An Introduction to Numerical Solution of the Navier-Stokes Equations," AIAA Paper 75-1, Jan. 1975.

[10] Bartlett, E.P. and Kendall, R.M., "Non-Similar Solution of the Multi-Component Laminar Boundary Layer by an Integer Matrix Method," NASA CR-1062, March 1967.

[11] Howey, D., Siegelman, D., and Lin, T.C., "Carbon-Carbon Nosetip Development Program Post-Test Summary Report," Avco Systems Div., AVSD-0363-75-RR, Dec. 1975.

[12] Schmidt, H., "Status Report on the Calculation of Blunt Body Flow Fields in Supersonic, Non-uniform Flows," Arnold Engineering Development Center, AEDC-TR-76-31, March 1976.

[13] Moretti, G. and Salas, M.D., "Numerical Analysis of the Viscous Super-sonic Blunt Body Problem, Part I," Polytechnic Inst. of Brooklyn, PIBAL Rept. 70-58, Nov. 1970; also AIAA Paper 69-139, 1969.

[14] Widhopf, G.F. and Victoria, K.J., "Numerical Solution of the Unsteady Navier-Stokes Equations for the Oscillatory Flow over a Concave Body," *Fourth International Conference on Numerical Methods in Fluid Dynamics,* Boulder, Colo., June 24-28, 1974.

[15] Behrens, W., "The Far Wake Behind Cylinders at Hypersonic Speeds, Part I. Flow Field," *AIAA Journal,* Vol. 5, Dec. 1967, pp. 2135-2144.

[16] Reeves, B.L., "Analysis of Unsteady Flow Separation over Severely Indented Nosetips," Avco Systems Div., SAMSO-TR-75-269, Vol. VI, Wilmington, Mass., Sept. 1975.

[17] Holden, M.S., "Experimental Studies of Separated Flows at Hypersonic Speed, Part I: Separated Flows over Axisymmetric Spiked Bodies," *AIAA Journal,* Vol. 4, April 1966, pp. 591-599.

[18] Donaldson, C.D. and Snedeker, R.S., "A Study of Free Jet Impingement, Part I. Mean Properties of Free and Impinging Jet," *Journal of Fluid Mechanics,* Vol. 45, Jan. 1971, pp. 281-319